From bad electrochemical practices to an environmental and waste reducing approach for the generation of active hydrogen evolving electrodes

Lisa Ring[a], Bruno G. Pollet[b], Marian Chatenet[C], Sofyane Abbou[c], Karsten Küpper[d], Mercedes Schmidt[a], Marten Huck[a], Aurelia Gries[a], Martin Steinhart[a], and Helmut Schäfer[a*]

[a]Institute of Chemistry of New Materials, University of Osnabrück, Barbarastrasse 7, 49076 Osnabrück, Germany

[b]Hydrogen Energy and Sonochemistry Research group, Department of Energy and Process Engineering, Faculty of Engineering, Norwegian University of Science and Technology (NTNU) NO-7491, Trondheim, Norway

[c]Univ. Grenoble Alpes, CNRS, Grenoble-INP (Institute of Engineering, Univ. Grenoble Alpes), LEPMI, 38000 Grenoble, France

[d]Department of Physics, Universität Osnabrück, Barbarastrasse 7, 49076 Osnabrück, Germany

*Email: helmut.schaefer@uos.de

Abstract: The electrodeposition of noble metals using corresponding dissolved metal salts represents an interesting process for the improvement of the electrocatalytic Hydrogen Evolution Reaction (HER) properties of less active substrate materials. The fact that only a small fraction of the dissolved noble metals reaches the substrate represents a serious obstacle to this common procedure. We therefore chose a different path. It was found that the HER activity of Ni42 alloy drastically increased (□= 140 mV at j=10 mA/cm^2; pH1) when a platinum counter electrode was used during polarization experiments in acid. This improvement was caused by a platinum transfer from the platinum anode to the steel cathode, a process which occurred simultaneously to the hydrogen evolution. The negligible accumulation of Pt (26 µg) in the electrolyte makes this straight-forward transfer procedure to a highly cost-effective, environmentally friendly, and waste reducing approach for the generation of cheap, stable and

effective HER electrodes.

Introduction

The ever-growing global energy demand of future societies can, in harmony with the environment, only be fulfilled by sustainable energy sources like sunlight, wind and thermal. Solar energy can be stored in "chemical bonds". This can be reasonably achievable via water electrolysis using either a Proton Exchange Membrane Water Electrolyzer (PEMWE) or an Alkaline Water Electrolyzer (AWE) leading to the so-called solar fuels [1,2,3,4,5,6,7,8,9] which in this case consists of generating hydrogen (H_2), a promising energy carrier[5] and oxygen (O_2).

Although hydrogen offers many advantages over other fuels, the cost for producing electrolytic hydrogen is rather high, with a current production price of €5-10/kg[10]. This price is related to the cost of electricity, and should be considered in addition to the capital cost (CAPEX) and operational cost (OPEX) of the electrolyzer; as most of PEMWEs use Platinum Group Metals (PGMs) such as iridium (Ir) and platinum (Pt), the PEMWE technology is inherently costly. PGMs and in particular Pt is used as it is the most effective electrocatalysts for the HER [11,12]. However, whilst Pt is characterized by its high-performance (low overpotential towards the HER), the metal is very expensive and thought to be scarce. Thus, there is still a need for developing cheap and easily accessible electrode materials that exhibit low overpotentials on the cathode side, allowing for efficient conversion of electrical energy into hydrogen gas through the HER.

The electrodeposition of a thin, highly HER active Pt layer on a conductive substrate represents one possible route on the way to such a desired material.

The conventional approach to electrodeposit Pt takes advantage of a Pt containing electrolyte

achieved upon the dissolution of Pt salts. From experience, it has been observed that only a very small fraction of the platinum originally dissolved is transferred to the electrode (intended to be modified), which definitely lowers the cost- efficiency and the environmental friendliness of this approach. In our conditions we have been following a different path allowing the decoration of Pt on stainless steel using a Pt counter electrode (CE) and a Ni42 steel working electrode (WE) in a water electrolysis reaction carried out at a low pH value and in an electrolyte not containing any Pt salts initially.

Generally, the use of a platinum CE for the evaluation of non-PGM based electrodes is well-known to be questionable, due to the risk of contaminating the WE with platinum especially when positive potentials are applied to the Pt electrode [13]. However, in this work, we used this drawback to our advantage. Upon using this strategy (self-dissolution of Pt at high electrodepotential e. g. E> +1600 mV *vs*. RHE) we could only detect a negligible amount of remaining platinum in the electrolyte used clearly underpinning the 100% effectiveness of the platinum transfer process. The simultaneously occurring hydrogen evolution on the Ni42 stainless steel surface affected the electrodeposition of a homogeneous layer but was substantially suppressed upon applying ultrasonic energy (80 kHz, 48-72 W) to the electrolysis cell (the setup of which is shown in Figure 1). The decoration of Ni42 stainless steel with Pt via the ultrasonic and sonoelectrochemical approaches were found to be highly effective to render steel in a competitive hydrogen-evolving electrode without exhibiting the disadvantage of classically performed Pt decoration processes: The wastage of expensive platinum.

Figure 1. Photo of the experimental setup taken before carrying out the polarization experiments in the absence and presence of ultrasound (a) and whilst performing the first activation procedure (b).

Results and Discussion

Silent conditions

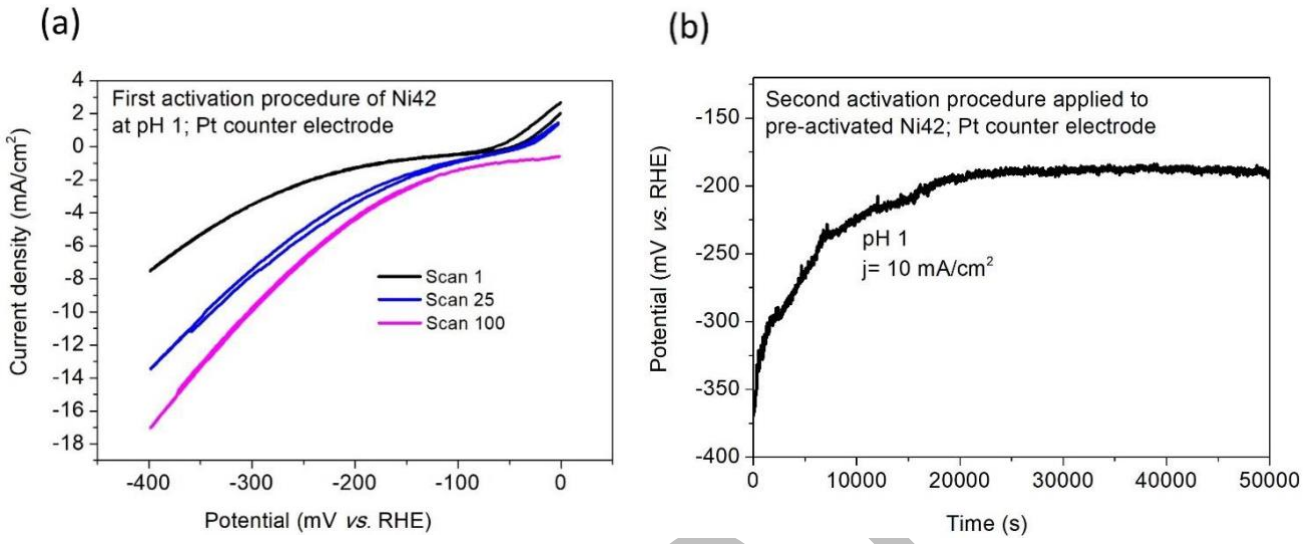

Figure 2. Electrochemical activation of Ni42 steel upon usage of a Pt counter electrode. **2(a**) First activation procedure based on a cyclic voltammetry experiment. **2(b**) Second activation procedure based on a chronoamperometry experiment.

Recently Schäfer and Chatenet showed that surface-modified (stainless) steel can be used as water splitting electrodes [14]. The approaches shown by Chatenet *et al* [15]. and Schäfer *et al*. [16,17,18,19] and by some of other groups are taking advantage of the elements contained in steel like Fe, Ni and Co, known for their good sophisticated properties (at least) towards the electrocatalytically-initiated OER. However, scientists failed, likely due to the absence of noble ingredients, in rendering steel at least as active for the HER than Pt is[14].

In this study, electrochemical decoration of Ni42 stainless steel with platinum was realized in 0.05 M sulfuric acid (initially free of any dissolved Pt species) by using a three-electrode set up consisting of a

stainless steel Ni42 WE, a platinum CE and a reversible hydrogen electrode (RHE) as reference electrode (Figure 1). Platinum was transferred from the CE to the WE via a procedure consisting of repeated cycling (100 cycles) in the potential (E) range 0.00 V *vs.* RHE and -0.40 V *vs.* RHE (E of the Pt

CE was at most +1.70 V *vs.* RHE), followed by a galvanostatic long-term polarization procedure (Figure 2), resulting in Pt decorated Ni42 stainless steel henceforth referred to as "sample Ni42Pt".

Figure 2 (a) shows that larger currents to potential ratio are obtained upon cycling of the potential. After 100 voltammetry cycles, the current density reached -17 mA/cm^2 at a potential of E=-400 mV *vs.* RHE, a value that is ca. 2.5 times higher than that observed for untreated Ni42 (~7 mA/cm^2, Figure 2a).

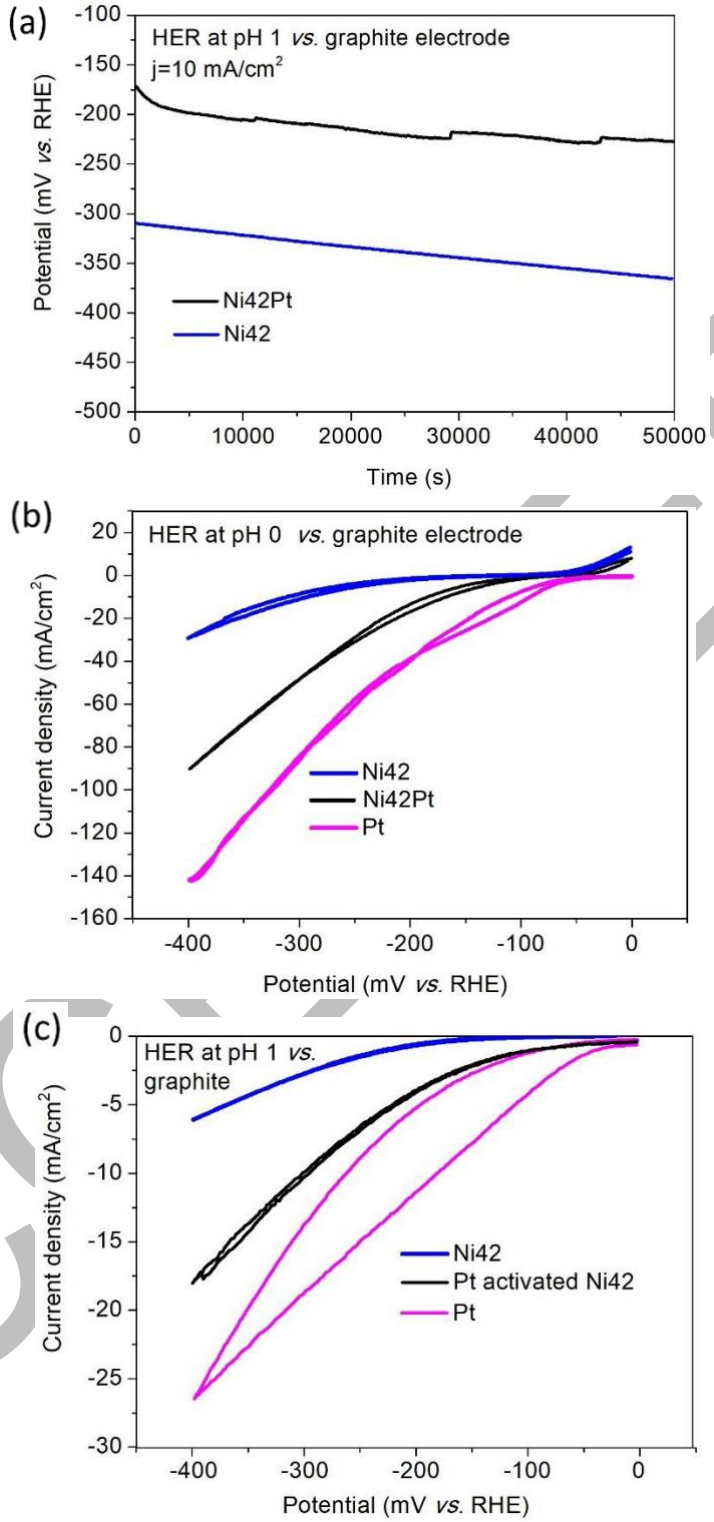

Figure 3. The electrochemical HER properties of Ni42 stainless steel decorated (or not) with Pt at pH0 and pH1 evaluated upon usage of graphite as counter electrode and compared with noble HER benchmarks. (**a**): Comparison of the steady state HER performance (pH1) of samples Ni42 and Ni42Pt. (**b**): Comparison of the non-steady state HER performance (pH0) of platinum with samples Ni42 and Ni42Pt. (**c**) Comparison of the non-steady state HER performance (pH1) of platinum with

samples Ni42, and Ni42Pt.

This was confirmed under steady state conditions as the potential required to ensure -10 mA/cm$_2$ current density decreased by 180 mV (from 370 mV overpotential to 190 mV overpotential) through 50000 s of chronopotentiometry (Figure 2(b). The contamination of a non-PGM-based working electrode by a Pt counter-electrode is a classical issue in electrocatalysis [12]. Thus, it was an indispensable pre-requisite to replace the platinum counter electrode with a material that does not lead to any contamination of the working electrode, for example, graphite (Figure 3).

In comparison with non-activated Ni42 steel, Ni42Pt exhibited a substantial enhancement in HER activity (Figure 3, black and blue curves) at pH1 and pH0. The average potential after 50,000 s of chronopotentiometry was found to be -218 mV *vs.* RHE (j = -10 mA/cm$_2$; 0.05 M H_2SO_4, Figure 3(a), black curve) whereas non-treated Ni42 steel required an average potential of E=-335 mV *vs.* RHE (Figure 3(a), blue curve).

The HER based current density realized at potential of E=-400 mV *vs.* RHE was found to be -30 mA/cm^2 for pH0 and -6 mA/cm$_2$ for pH 1 for the non-treated Ni42 samples and, -90 mA/cm$_2$ for pH 0 and -17.5 mA/cm$_2$ for pH1 for the sample Ni42Pt (Figures 3(b) and 3(c)). In any case, there is still a significant difference in overall HER performance at pH 0 or 1 between pure Pt (determined by us or other groups[20, 21]) and sample Ni42Pt (Figures 3(b) and 3(c)) as can be taken from the substantial gap between the CV curves of samples Pt and Ni42Pt recorded at pH1 and pH0 (Figures 3(b) and 3(c)). In addition, and in our conditions, a substantial decrease of the HER activity for sample Ni42Pt under long-term measurements was observed (Figure 3(a), black curve). For example the potential was found

to increase by ~+80 mV after 50,000 s of chronopotentiometry carried out in 0.05 M sulfuric acid at *j* = -10 mA/cm$_2$ (Figure 3(a), black curve). From these observations, it can be stipulated that two processes occur simultaneously on the surface of Ni42 steel during the first and second activation procedures (Figure 2), namely hydrogen (H_2) bubble formation and Pt electrodeposition [22].

Moreover, it turned out that the shift of the CV curves towards higher current density values with increased number of cycles (up to 100) as seen in Figure 2(a), can only be achieved when the electrolyte volume, the magnetic stirring bar size, the stirring speed and the electrode geometry (*i.*e. the distance between the Ni42 working electrode and the Pt counter electrode, and the distance between Ni42 and the reference electrode) are optimized. If too "strong" stirring is used, Pt species cannot diffuse/migrate from the Pt anode (counter electrode in OER and dissolution regime) to the Ni42 cathode (working electrode, in HER and Pt deposition regime). If, on the other hand, the stirring is too "weak", H_2 bubbles are not released fast enough from the Ni42 working electrode surface and may affect the electrodeposition of Pt species.

Ultrasonic conditions

In order to overcome and circumvent these problems, ultrasonication (80 kHz, 48-72 W) was used. Ultrasonic applied to electrochemically promoted reactions is known to influence not only gas bubble removal from surfaces but offers many advantages [23, 24]. An increase in electrode cleanliness, metal depassivation, enhanced mass-transport of electroactive species to the electrode surface will result in enhanced electrochemical diffusion processes, in an increase in (a) electrochemical rates and yields, (b) process efficiencies, as well as in a decrease of electrode overpotentials; this overall leads to improved electroplated and electrodeposited materials (hardness, porosity and thickness) [25].

We would like to emphasize at this point that we employed ultrasound solely for the fabrication of the

HER electrode and not when the ready-made electrode was used as a hydrogen forming electrode. Thus, we would like to address questions whether ultrasound affects *e.g.* electron transfer kinetics[23] in an additional contribution.

Ultrasonic-assisted two steps cyclic voltammetry activation followed by ultrasonic-assisted chronopotentiometry was applied to Ni42 (see supplementary information), both performed using a platinum counter electrode (Figure 4).

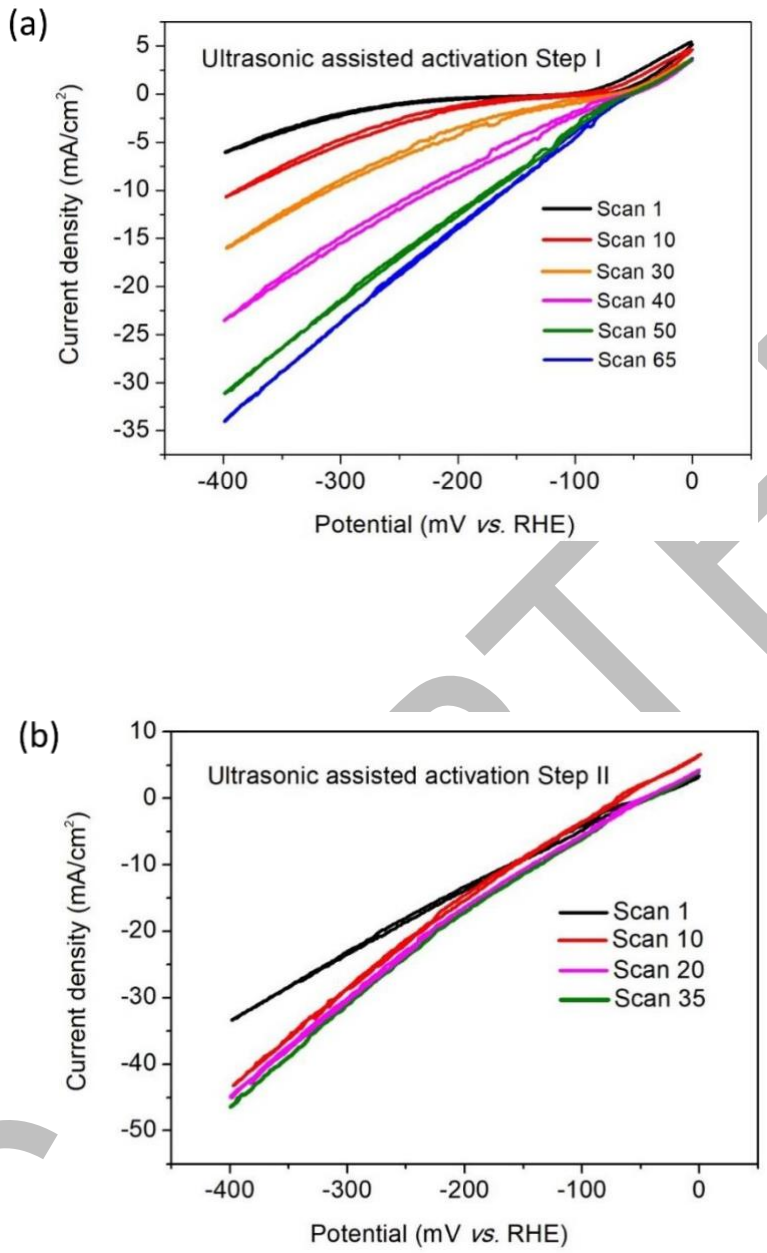

Figure 4. Ultrasonically-assisted electrochemical activation of Ni42 stainless steel upon usage of a Pt counter electrode; Ultrasonic frequency: 80 kHz. **(a)** First activation procedure consisting of ultrasonically-assisted (80 kHz, 48 W) 65 cyclic voltammetry scans. **(b)** Second activation procedure consisting of ultrasonically-assisted (80 kHz, 72 W) 35 cyclic voltammetry scans.

Whereas 100 CV cycles were required in the absence of ultrasound to reach a current density of ~-17 mA/cm$_2$ (Figure 2(a), this value was obtained after only 30 CV cycles when the electrolysis cell was

under ultrasonic treatment (80 kHz, 48 W) (Figure 4(a)). After 65 CV scans (j=-34 mA/cm^2 at E=-400 mV *vs.* RHE) ultrasonic-assisted activation step I), an intermediate step was added to clean the platinum

electrode for 60 min in a water ultrasonic bath, before polarization experiments were continued (ultrasonically-assisted activation step II; 80 kHz, 72 W Figure 4(b)). The current density reached -46 mA/cm^2 after further 35 CV scans (Figure 4(b)). An additional step (ultrasonic assisted activation step III) consisting of ultrasonically-assisted chronopotentiometry performed in the presence of a Pt counter electrode which ends up in sample Ni42SoPt, turned out to be efficient in order to improve the stability of the HER catalyst (Supplementary information; Figure (S1)). Long-term polarization experiments with a graphite counter electrode reveal Ni42SoPt as a highly active and highly stable HER electrode in an acidic medium (Figure 5a).

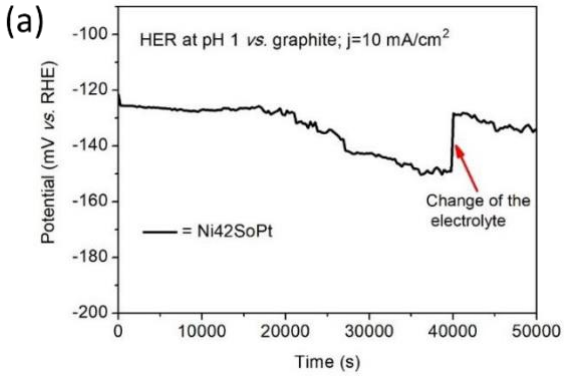
(a)
HER at pH 1 vs. graphite; j=10 mA/cm2
Potential (mV vs. RHE)
-100
-120
-140
-160
-180
-200
0
10000
20000
30000
40000
50000
Time (s)
Change of the electrolyte
= Ni42SoPt

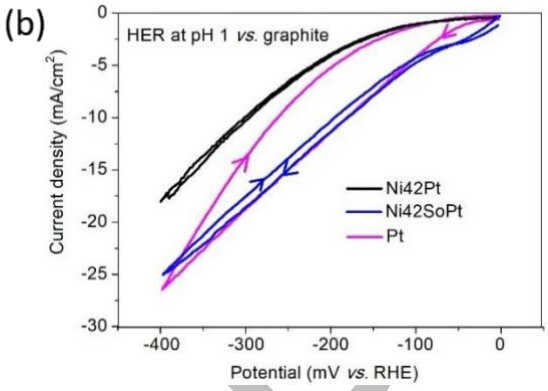
(b)
HER at pH 1 vs. graphite
Current density (mA/cm2)
0
-5
-10
-15
-20
-25
-30
-400
-300
-200
-100
0
Potential (mV vs. RHE)
Ni42Pt
Ni42SoPt
Pt

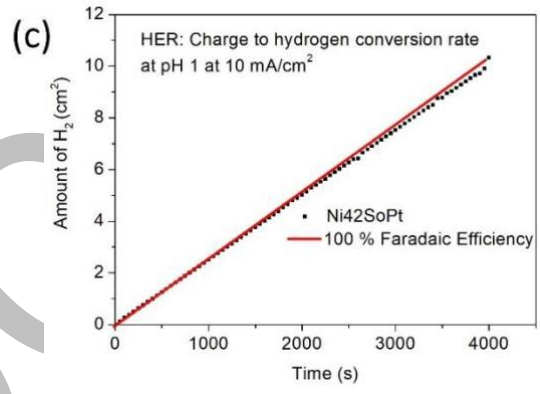
(c)
HER: Charge to hydrogen conversion rate
at pH 1 at 10 mA/cm2
Amount of H2 (cm2)
12
10
8
6
4
2
0
0
1000
2000
3000
4000
Time (s)
Ni42SoPt
100 % Faradaic Efficiency

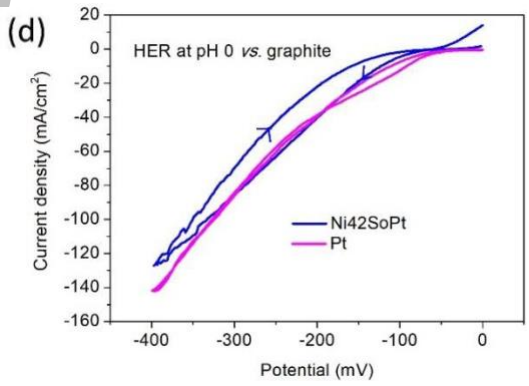
(d)
HER at pH 0 vs. graphite
Current density (mA/cm2)
20
0
-20
-40
-60
-80
-100
-120
-140
-160
-400
-300
-200
-100
0
Potential (mV)
Ni42SoPt
Pt

Figure 5. The HER performance of sample Ni42SoPt determined versus a graphite electrode. **(a)** The steady state HER performance (pH1) of Ni42SoPt. **(b)** The non-steady state HER performance (pH1) of Ni42SoPt. **(c)** Determination of the charge to hydrogen conversion rate for the HER on sample Ni42SoPt based on a chronopotentiometry scan. The red line corresponds to 100% Faradaic efficiency (FE). The FE determined after 4000 s amounted to 99.9%. **(d)** Comparison of the non-steady state HER performance (pH0) of platinum with sample Ni42SoPt.

Sample Ni42SoPt exhibits the best electrocatalytic HER properties of all platinum-activated Ni42 samples. Exhibiting a current density of j=-25 mA/cm^2 at -400 mV *vs.* RHE (Ni42Pt, j = -17.5 mA/cm^2), Ni42SoPt outperforms sample Ni42Pt and was found to be nearly *on par* with the one for pure platinum (j = -26.3 mA/cm$_2$; Figure 5(b)). A quantitative charge to hydrogen conversion rate (99.9%) was determined for the electrocatalytically-initiated hydrogen evolution upon sample Ni42SoPt (Figure 5(c)); see supplementary information). A potential industrial implantation of our Ni42SoPt electrode (PEM electrolyzer with 120 cells each of them 20 x 20 cm) with a total electrode area of 4.8 m$_2$, would theoretically result in a production rate of 6.14 m$_3$H$_2$/h at 20 °C, at j= 300 mA/cm$_2$ and FE=95 %. As expected, sample Ni42SoPt exhibited, not only in 0.05 M H_2SO_4 but also in 0.5 M H_2SO_4, a very close HER performance (E= -400 mV *vs.* RHE at j = -125 mA/cm^2) compared to pure platinum (sample Pt; E= -400 mV *vs.* RHE at j = -140 mA/cm$_2$; Figure 5(d). In the high current density range (-10 < j < -150 mA/cm^2), a *Tafel slope* was found to be 191 mV dec^{-1} (Supplementary information; Figure (S2)). The *Tafel slope* for Pt in the same current density region amounted to 109 mV dec$_{-1}$ (Ni42: 201 mV dec$_{-1}$; Ni42Pt: 206 mV dec^{-1}; Supplementary information; Figure (S2)). Pure platinum shows better HER

performance at high current densities than Ni42SoPt does. We claim that the differences in Tafel slopes are due to different physicochemical properties of the surfaces (e.g. hydrophobicity, porosity) which influence bubble adhesion/detachment. However, the HER performance (under laboratory conditions) can be seen as competitive to recently-developed electrocatalysts[26, 27] as well as commercially available ones[28,29]. For example, Popczun *et al.*[27] recently reported that nano-scaled Ni_2P exhibited highly-active and stable electrocatalytically initiated hydrogen evolution. In their conditions, Ni_2P

nanoparticles were synthesized in high boiling organic solvent (1-octadecene, oleylamine and tri-n-octylphosphine) and deposited on titanium foil with a catalyst (Ni_2P) loading of 10 µg/mm_2. The potential required for j=-10 mA/cm_2 HER based current density derived from steady-state measurements amounted to -115 mV *vs.* RHE in 0.5 M sulfuric acid. A flat electrode consisting of metal ion containing triazine thiolate modified copper was recently introduced by Vishwanath *et al* [30]. and turned out to be substantially weaker (HER-) active (E= −270 mV *vs.* RHE at *j*=-10 mA/cm_2 in 0.5 M H_2SO_4) than our modified stainless steel. Co_2P nanowires generated upon a microwave-assisted approach showed at given potential, competitive current densities (E= -110 mV *vs.* RHE at *j* = -10 mA/cm^2) [31]. Based on Tafel measurements Ma et al. determined for commercial Pt/C with a loading of around 50 µg/cm_2, at □ □ 35 mV a HER based current density of -1.6 mA/cm_2 [28] which represents an activity below the one of Ni42SoPt (j= -7 mA/cm_2 at □ = 40 mV; Figure S2). In addition it should be mentioned at this point that in contrary to our steel-based electrodes, Pt/C as well as the electrode consisting of Co_2P nanowires cannot be seen as a flat one, leading to a projected surface area significantly lower than the real surface area; so, the high current density monitored cannot be directly compared with those derived from flat electrodes. This also explains why the overpotential at given current densities reported in some contributions for porous materials is even lower than the one that is assigned to pure platinum. Thus, the HER onset potential seems to be a more meaningful HER activity parameter and here platinum (smooth) metal still can be seen as the benchmark [32]. With respect to the onset of hydrogen evolution (E_{onset}= potential to ensure a HER based current density of -0.25

mA/cm^2) in pH 1 regime our modified steel Ni42SoPt is highly competitive (-14 mV *vs.* RHE) to platinum metal (-12 mV *vs.* RHE; Figure 5(b), 5(d), Table 1) and substantially better than samples Ni42 (E_{onset}= -

To sum up: Whereas under laboratory conditions (current density up to 50 mA/cm^2) Pt modified Ni42 steel is on par with Pt (Figure 5) under industrial conditions (j>50 mA/cm$_2$) there is still a gap 160 mV *vs.* RHE) and Ni42Pt (E_{onset} =-32 mV *vs* RHE).

between Ni42SoPt and pure Pt (Figure S2).

Different coatings (Nickel-iron alloy, SiO_2, TiO_2, ZrO_2, AlOOH) applied to steel aiming in the improvement of its HER properties have been described in the literature[33,34]. However, the studies lack long-term stability measurements. Relatively recent studies exhibited HER activities which are far away from those observed using PGM[35]. In addition, to the best of the authors' knowledge, the majority of approaches shown in the literature focuses on the development of active and durable HER electrodes in alkaline media when PEMWEs[35,36,37,38] require OER and HER electrodes that are active and stable at low pH values. In particular the stability criteria at low pH is difficult to reach; thin layers of PGMs deposited on steel are however known to significantly improve the corrosion resistance of steel due to passivation[39].

In order to shed further light on the HER mechanisms on our *as*-prepared electrodes and confirm successful decoration of Pt on Ni42 steel, we investigated the surface of Ni42SoPt by means of SEM (Figures 6 (a, b, c and d)) and AFM (Figure 6(e)). Top view SEM (Figure 6(a)) and AFM (Figure 6(e)) images confirmed that the roughness of Ni42 steel (average roughness 71.5 nm)[40] was not substantially increased upon the chosen surface modification (Ni42SoPt: 98 nm). Double layer capacity investigations have been carried out with samples Ni42, Ni42Pt and Ni42SoPt (see supplementary information Figures S3-S8.). An unusual high double-layer capacitance was determined for all samples (Ni42: 6.8 mF cm^{-2}, Ni42Pt: 2.7 mF cm^{-2}, Ni42SoPt: 4.35 mF cm^{-2}). Values in the mF/cm^2 range were also obtained for surface modified S235 steel as reported by us in one of our previous contributions [41]. However, phosphorized S235 steel exhibited substantially higher double-layer capacitance values (46.1 mF cm^{-2}) than untreated S235 steel did (0.2 mF cm^{-2})[41], which was very likely caused by the enormous

increase of the porosity that occurs to steel S235 when phosphorized at high temperatures. Thus, we stipulate that the double layer capacitance values derived from samples Ni42, Ni42Pt and Ni42SoPt, which are of the same order of magnitude, basically result from comparable roughness of samples Ni42, Ni42Pt and Ni42SoPt; this is confirmed by AFM and SEM techniques (Figure 6). Table 1 gives an overview of the electrochemical properties of samples Ni42, Ni42Pt, Ni42SoPt and platinum; derived from non-steady-state and steady-state HER based measurements; it also compares the AFM results

of samples Ni42, Ni42Pt and Ni42SoPt. Elemental analysis of the surface of sample Ni42SoPt was obtained by X-ray energy-dispersive spectroscopy (XEDS; Figure (6a-d)), and X-ray photoelectron spectroscopy (XPS; Figure 6(f)), respectively. Both methods confirmed the existence of Pt on the surface of sample Ni42SoPt; it was also observed that not only elemental platinum was found on the surface of sample Ni42SoPt: in addition to Pt_0, platinum in oxidation state +2 was revealed (Figure 6(f)). A similar finding was recently reported by Yuan et al.[42].

The Pt 4f core level XPS consists of two peaks located at 71.3 ($4f_{7/2}$) and 74.6 eV ($4f_{5/2}$) on a binding energy scale. Whereas the $4f_{7/2}$ core level energy is expected to be located at 70.7 eV for the metallic Pt "bulk" state of a polycrystalline Pt foil[43], binding energies of 71.0 eV to 71.3 eV have been obtained for Pt electrodes with the platinum being in polycrystalline and nanostructured form[44, 45]. The features, which we associate to metallic Pt (blue), show a rather pronounced tail (asymmetry) to higher binding energies (Figure 6(f)), another strong indication for metallicity. The analysis of the peak areas after background subtraction reveals that the platinum at the surface of sample comprises around 94.5% metallic Pt (blue) and 5.5% can be attributed to $Pt(OH)_2$ (green). The Pt 4f7/2 binding energy of 72.2 eV found from the deconvolution for $Pt(OH)_2$ is in excellent agreement with the result for chemisorbed O/OH on Pt reported by Saveleva et al.[45]

These findings made the authors believe that platinum-oxide species are formed on the Pt counter electrode whilst HER on Ni42, for a given cell voltage of ~2.1 V (Pt: Anode and Ni42: Cathode), at $E_{cathode}$= -400 mV *vs.* RHE (E_{anode}=+1700 mV *vs.* RHE). Thus, oxygen evolution took place on the Pt surface. Pioneering studies by the groups of Hoare, Bard, Bockris, and several others [46, 47, 48] showed

that the cell voltage required to produce oxygen on a metallic surface is related to the redox potential of the metal/metal oxide couple, or in other words, even in the case of noble metals no oxygen can be released from the surface if the corresponding metal oxide is not formed.

(a)

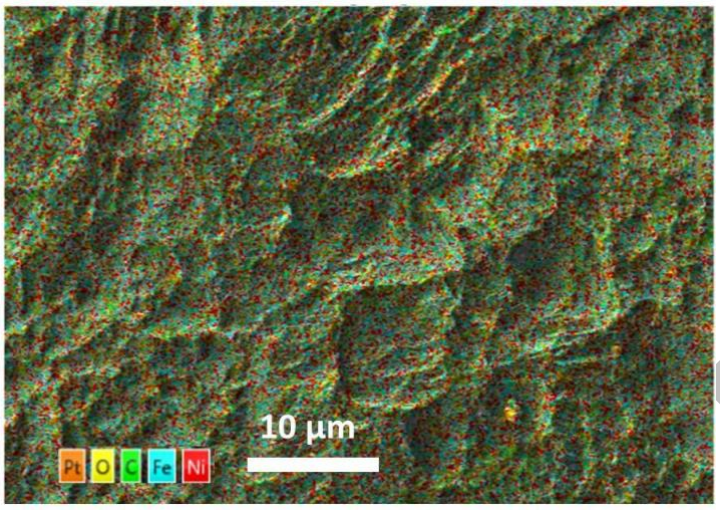

(b)

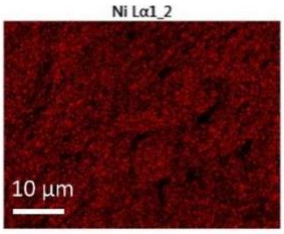

(c)

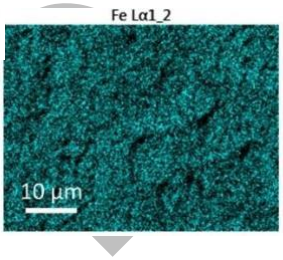

(d)

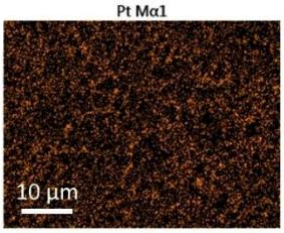

(e)

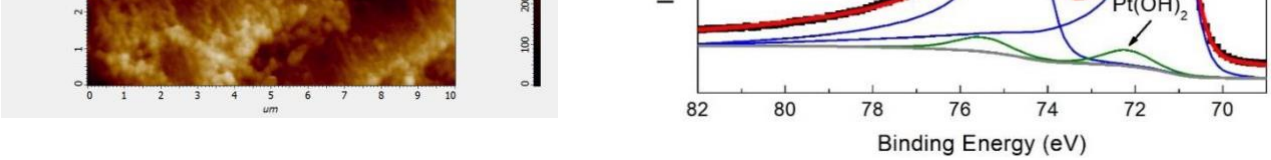

Figure 6. SEM, AFM and XPS results of sample Ni42SoPt. Overlay image of a SEM picture with EDS data; *Layered image combining 5 (Ni, Fe, Pt, O, C) maps* **(a)**. EDS maps of Ni **(b)**, Fe **(c)** and Pt **(d)**. AFM image of sample Ni42SoPt Sampling area: 100.062 um*um. Height parameters: Root mean square roughness: 123.8 nm; Average roughness: 97.96 nm; Area peak-to-valley height: 902.1 nm; Maximum area peak height: 430.4 nm; Maximum area valley depth: 471.7 nm; Projected area: 100.062 μm^2; Surface area: 131.4 μm^2 **(e)**. High resolution Pt 4f x-ray photoelectron spectrum of sample Ni42SoPt (black points). The red line represents the result of the optimized fit. The de-convolution resulted in two $4f_{7/2}$ peaks located at 71.3 eV (Pt^0)[45] and 72.2 eV ($Pt(OH)_2$)[45], and two $4f_{5/2}$ peaks located at 74.6 eV (Pt^0) and 75.6 eV ($Pt(OH)_2$) binding energy, respectively **(f).**

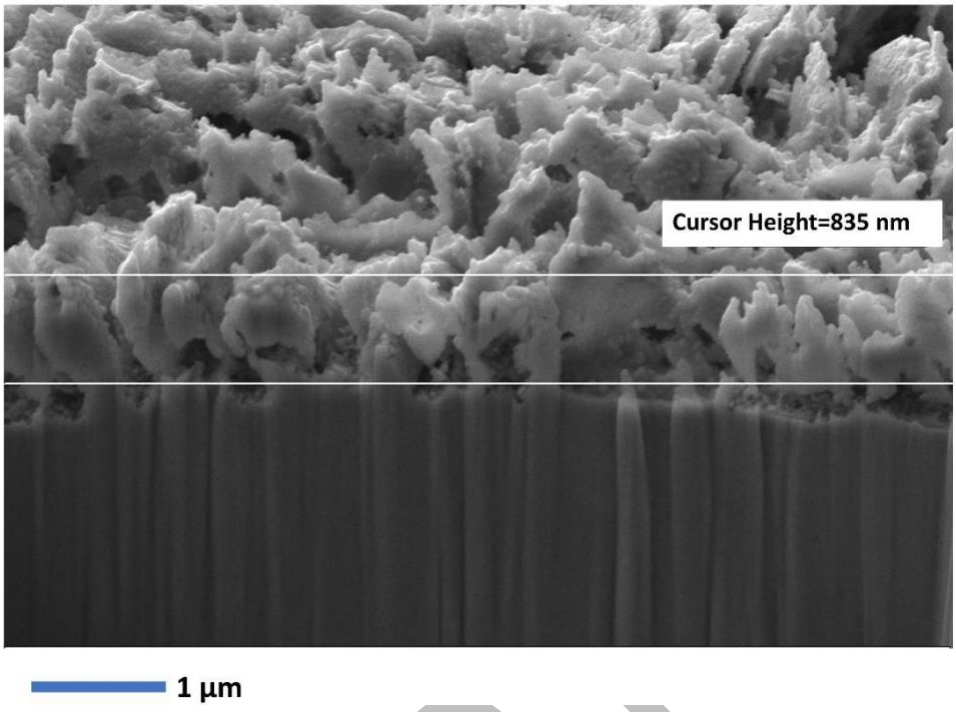

Figure 7. SEM micrograph of a FIB machined cross section of sample Ni42SoPt. The rear wall of the trapezoidal trough is shown. This wall is orientated perpendicular to the surface of the specimen thus presenting a cross section of the sample. The accelerating voltage was adjusted to 7 kV and the SEM images were acquired using a secondary electron (SESI). Ion (Ga) beam settings: current: 240 pA, voltage: 7 kV, duration: 25 min.

Thus, it is reasonable to assume that platinum oxide (PtO) is formed on the surface of the Pt counter electrode during the activation procedure leading to sample Ni42SoPt. Indeed, at potentials higher than +1 V vs. RHE in dilute sulfuric scid, Pt initiates its surface (and then bulk) oxide formation, as well documented by the seminal work of Conway *et al.* [49,50,51,52]. We herein claim that platinum oxide species formed on the Pt anode may be dissolved in the H_2SO_4 and cationic Pt oxide species can be electrodeposited on the Ni42 steel (Figure 6(f)). This assumption seems to be founded [53,54,55] for example, Mitsushima *et al.* [53] investigated the dissolution of Pt in the presence of O_2 in sulfuric acid and postulated the following dissolution reaction:

$$PtO_2 + H^+ + H_2O \rightarrow Pt(OH)_3^+ \quad (1)$$

The thickness of the Pt layer after the ultrasonically-assisted activation steps I-III as determined by cross-sectional analysis amounted to ca. 800-900 nm (Figure 7). Taking into account, the density of platinum of 21.45 g/cm^3 and

the electrode area of 2 cm_2, the total amount of platinum deposited on the Ni42 surface was calculated to be 3.65 mg based on a (fully) compact layer which agrees well with the mass loss of the Pt counter electrode that occurs whilst sample preparation. Based on five sample (Ni42SoPt) preparations the average mass loss of the Pt counter electrode amounted to 2.94 mg (for each sample produced) and the sum of the amount of Fe, Ni and Pt dissolved in the electrolyte determined by ICP-MS technique was found to be 2.81 mg (Table 2). Notably: The extremely low amount of Pt (26 µg) in 100 mL of electrolyte. Thus, only 0.88% of the 2.94 mg Pt (Pt mass loss of the CE) accumulates in solution, the rest is deposited. At first glance the absence of a mass increase of the Ni42 electrode during deposition (mass change: -3.22 mg) seems to be unusual. The analysis of the electrolyte reveals that the amount of Pt which is added to the Ni42 substrate (3.65 mg as mentioned above) is compensated by dissolution of Fe and Ni (Table 2). The Pt-decoration process is therefore likely (at least to some extent) to be a cementation (electroless) process, in which Pt^{II} species originating from the counter-electrode dissolution, play the role of oxidant at the Ni42 surface, leading to the preferential dissolution of Ni^{II} or Fe^{II}/Fe^{III} species (e.g. $Pt^{II}+Ni \rightarrow Ni^{II} + Pt$). The Pt loading (ca. 18 µg/mm^2) is still below the lower limit compared to the loading of some commercially available electrodes[28,29,56] as Pt and Ir loadings in state-of-the art electrolysers are in the range of 2–5 mg cm^{-2}. For instance the loading for platinum black coated Nafion®115 from FuelCellsEtc used as cathode for PEMWE type electrolyzers amounts to 30 µg/mm^2. [7] Recent studies have shown that lower Pt loadings can be feasible [57]. However, while Pt/C electrodes are inherently rather immune in HER conditions, this might not be the case when the electrolyzer operates in “start/stop” mode; in these conditions, the “hydrogen electrode” would likely sweep between negative potentials (versus the RHE) in operation, and potentials as high as ca. +1 V *vs*. RHE in stop (in that case, air would likely intrude the whole cell). Alternation of the electrode potential on Pt/C electrocatalysts can be very detrimental, as Pt nanoparticles can catalyse the local corrosion of the carbon substrate, leading to restructuration

of the active layer and loss of Pt nanoparticles (and of electrochemical surface area)[58, 59, 60, 61, 62]. Such processes have been thoroughly studied for proton exchange membrane fuel cells [63, 64], and until now, been roughly disregarded in PEMWE. This could be a serious issue for PEMWE operated for the storage of renewable electricity (the present endeavour), and that the present solution brought by the authors (it is a carbon-free material), must not be subjected to such degradation.

Sample	Onsetpotential derived from cyclic-voltammetric measurements at j=-0.25 mA cm^{-2}		Averaged Overpotential required for j=10 mA/cm^2 based on Chronopotentiometry measurements		Tafelslope pH 0 [mV dec^{-1}]	C_{dl} pH1 [mF cm^{-2}]	Projected area (PA) surface area (SA) and average roughness (AR) as derived from AFM
	pH 1	pH 0	pH 1	pH 0			
Ni42	-160 mV *vs.* RHE	-140 mV *vs.* RHE	335 mV	306 mV	328	6.8	PA=99.9 µm^2 SA=101.8 µm^2 AR=71.5 nm
Ni42Pt	-32 mV *vs.* RHE	-28 mV *vs.* RHE	218 mV	99 mV	326	2.7	PA= 100.062 µm^2 SA= 132.3 µm^2 AR= 98 nm
Ni42SoPt	-14 mV *vs.* RHE	-9 mV *vs.* RHE	140 mV	88 mV	291	4.35	PA= 100.062 µm^2; SA= 131.4 µm^2 AR=98 nm
Pt	-12 mV *vs.* RHE	-7 mV *vs.* RHE	122 mV	81 mV	148	-	-

Table 1. Overview of the steady state and non-steady state HER based electrochemical measurements as well as the results from AFM testing carried out with samples Ni42, Ni42Pt, Ni42SoPt and Pt.

I	II	III	IV	V
Average mass loss of the Pt electrode [mg]	Average mass change of the Ni42 electrode occurring whilst decoration with Pt	Amount of Pt deposited on the Ni42 substrate*	Amount of transition metal ions dissolved in the electrolyte	Total amount of material dissolved in the electrolyte
2.94 mg	-3.22 mg	3.65 mg	0.026 mg[Pt] 1.60 mg [Fe) 1.18 mg [Ni]	2.81 mg

Table 2. Determination of the average mass loss of the platinum electrode (column I) and the average mass change of the Ni42 electrode (column II) based on 5 sample preparations; Determination of the amount of Pt deposited on

the Ni42 steel based on the outcome of the FIB-SEM experiment (column III); Determination of the amount of ions dissolved in the electrolyte (column IV and V).

Conclusions

The use of a platinum counter electrode for the evaluation of non-PGM based electrodes is controversially discussed and questionable, due to the risk of contaminating the WE with platinum. However, such weak point of this experimental setup turned out to be of tremendous benefit for the generation of a highly active and stable HER electrocatalyst. We used a simple three-electrode-based polarization approach carried out in acid with stainless steel as cathode and platinum as counter electrode.

The hydrogen bubble formation plus electrodeposition of platinum were found to occur simultaneously on the surface of Ni42 steel upon carrying out repetitive CV scans in sulfuric acid. The HER disturbs homogeneous decoration of Ni42 steel with platinum. However, the latter is advantageous with respect to activity and stability of the generated HER electrode and can be achieved by ultrasonicating the electrolytic cell. An optimized electrolysis protocol allows the generation of a very active (= +140 mV at *j* = -10 mA/cm$_2$ and at pH 1) and stable steel-based hydrogen evolution electrode, which can be seen as highly cost-effective due to the low amount of used platinum (18 µg/mm$_2$). Remarkably: only a negligible amount of Pt (26 µg) was determined in the electrolyte used for the platinum transfer reaction which means that around 99% of the Pt that comes from the Pt counter electrode is deposited on the WE making this procedure to an ideal alternative to usually exploited strategies.

Funding sources

This research did not receive any specific grant from funding agencies in the public, commercial, or not-for-profit sectors.

Conflict of interest

The authors declare no conflict of interest.

Water splitting ◦ heterogeneous catalysis

References

[1] F. Le Formal, W. S. Bouree, M. S. Prevot, K. Sivula, *Chimia* **2015**, *69*, 789-798.
[2] T. R. Cook, D. K. Dogutan, S. Y. Reece, Y. Surendranath, T. S. Teets, D. G. Nocera, *Chem. Rev.* **2010**, *110*, 6474-6502.
[3] M. G. Walter, E. L. Warren, J. R. McKone, S. W. Boettcher, Q. Mi, E. A. Santori, N. S. Lewis, *Chem. Rev.* **2010**, *110*, 6446-6473.
[4] H. A. Gasteiger, N. M. Markovic, *Science* **2009**, *324*, 48-49.
[5] S. Baranton, C. Coutanceau, *Appl. Catal. B:Environmental* **2013**, *136-137*, 1-8.
[6] X. Sun, K. Xu, C. Fleischer, X. Liu, M. Grandcolas, R. Strandbakke, T. S. Bjornheim, T. Norby, A. Chatzitakis, *Catalysts* **2018**, *8*, 1-41.
[7] G. Yang, S. Yu, J. Mo, Z. Kang, Y. Dormann, F. A. List III, J. B. Green, S. S. Babu, F.-Y. Zhang, *J. Power Sources* **2018**, *396*, 590-598.
[8] V. Artero, M. Chavarot-Kerlidou, M. Fontecave, *Angew. Chem. Int. Ed.* **2011**, *50*, 7238 – 7266.
[9] V. R. Stamenkovic, D. Strmcnik, P. P. Lopes, N. M. Markovic, *Nat. Mater.* **2017**, *16*, 57-69.
[10] C. Jorgensen, S. Ropenus, *Int. J. Hydrogen Energy* **2008**, *33*, 5335-5344.
[11] J. Wang, W. Cui, Q. Liu, Z. Xing, A. M. Asiri, X. Sun, *Adv. Mater.* **2016**, *28*, 215-230.
[12] C. C. L. McCrory, S. Jung, J. C. Peters, T. F. Jaramillo, *J. Am. Chem. Soc.* **2013**, *135*, 16977-16987.
[13] J. G. Chen, C. W. Jones, S. Linic, V. R. Stamenkovic, *ACS Catal.* **2017**, *7*, 6392-6393.
[14] H. Schäfer, M. Chatenet, *ACS Energy Lett.* **2018**, *3*, 574-591.
[15] F. Moureaux, P. Stevens, G. Toussaint, M. Chatenet, *J. Power Sources* **2013**, *229*, 123-132.
[16] H. Schäfer, S. Sadaf, L. Walder, K. Kuepper, S. Dinklage, J. Wollschläger, L. Schneider, M. Steinhart, J. Hardege, D. Daum, *Energy Environ. Sci.* **2015**, *8*, 2685-2697.
[17] H. Schäfer, D. M. Chevrier, K. Kuepper, P. Zhang, J. Wollschlaeger, D. Daum, M. Steinhart, C. Heß, U. Krupp, K. Müller-Buschbaum, J. Stangl, M. Schmidt, *Energy Environ. Sci.* **2016**, *9*, 2609-2622.
[18] H. Schäfer, K. Kuepper, J. Koppe, P. Selter, M. Steinhart, M. R. Hansen, D. Daum, *ACS Catal.* **2018**, *8*, 10914–10925.
[19] H. Schäfer, K. Kuepper, M. Schmidt, K. Müller-Buschbaum, D. Daum, M. Steinhart, W. Han, J. Wollschläger, U. Krupp, P. Hou, J. Stangel, X. Liu, *Catal. Sci. Technol.* **2018**, *8*, 2104-2116.
[20] D. Voiry, M. Salehi, R. Silva, T. Fujita, M. W. Chen, T. Asefa, V. B. Shenoy, G. Eda, M. Chhowalla, *Nano Lett.* **2013**, *13*, 6222-6227.
[21] Y. Zhang, A. Thomas, M. Antonietti, X. Wang, *J. Am. Chem. Soc.* **2009**, *131*, 50-51.
[22] B. G. Pollet, E. F. Valzer, O. J. Curnick, *Int. J. Hydrogen Energy* **2011**, *36*, 6248–6258.
[23] B. G. Pollet, *Ultrason. Sonochem.* **2019**, *52*, 6-12.
[24] M. H. Islam, O. S. Burheim, B. G. Pollet, *Ultrason. Sonochem.* **2019**, *51*, 533-555.
[25] B. G. Pollet, Ed.; Power Ultrasound in Electrochemistry: From Versatile Laboratory Tool to Engineering Solution; John Wiley & Sons: Hoboken, NJ, USA, (2012).
[26] E. J. Poczun, C. G. Read, C. W. Roske, N. S. Lewis, R. E. Schaak, *Angew. Chem. Int. Ed.* **2014**, *53*, 5427-5430.
[27] E. J. Popczun, J. R. McKone, C. G. Read, A. J. Biacchi, A. M. Wiltrout, N. S. Lewis, R. E. Schaak, *J. Am. Chem. Soc.* **2013**, *135*, 9267-9270.
[28] Y.-Y. Ma, C.-X. Wu, X.-J. Feng, H.-Q. Tan, L.-K. Yan, Y. Liu, Z.-H. Kang, E.-B. Wang, Y.-G. Li, *Energy Environ. Sci.*, **2017**, *10*, 788-798.
[29] Z. Duan, M. Pi, D. Zhang, P. Zhang, J. Deng, S. Chen, *Int. J. Hydrogen*, **2019**, *44*, 16, 8062-8069.
[30] R. S. Vishwanath, S. Kandaiah, *J. Mater. Chem. A* **2017**, *5*, 2052-2065.

[31]Z. Jin, P. Li, D. Xiao, *Green Chem.* **2016**, *18*, 1459-1464.
[32]J. Hu, C. Zhang, X. Meng, H. Lin, C. Hu, X. Long, S. Yang, *J. Mater. Chem. A* **2017**, *7*, 5995-6012.
[33]E. R. Gonzalez, L. A. Avaca, A. Carubelli, A. A. Tanaka, G. Tremiliosi-Filho, *Int. J. Hydrogen Energy* **1984**, *9*, 689-693.
[34]K. C. Leonard, M. I. Tejedor-Anderson, M. A. Anderson, *Int. J. Hydrogen Energy* **2012**, *37*, 18654-18660.

[35]S. Wang, W. Li, H. Qin, L. Liu, Y. Chen, D. Xiang, *Int. J. Electrochem. Sci.* **2019**, *14*, 957-969.
[36] G. Cabello, M. F. Gromboni, E. C. Pereira, L. H. Mascaro, F. Marken, *Electrochim. Acta* **2017**, *235*, 480-487
[37]T. Zhang, K. Yang, C. Wang, S. Li, Q. Zhang, X. Chang, J. Li, S. Li, S. Jia, J. Wang, L. Fu, *Adv. Energy Mater.* **2018**, *8*, 1801690.
[38]J. M. Olivares-Ramirez, M. L. Campos-Cornelio, J. Uribe Godinez, E. Borja-Arco, R. H. Castellanos, *Int. J. Hydrogen Energy* **2007**, *32*, 3170-3173.
[39]A. Fones, G. Hatton, *Platinum Metals Rev.* **2014**, *58*, 54-57.
[40]H. Schäfer, D. M Chevrier, P. Zhang, J. Stangl, K. Müller-Buschbaum, J. D Hardege, K. Kuepper, J. Wollschläger, U. Krupp, S. Dühnen, M. Steinhart, L. Walder, S. Sadaf, M. Schmidt, *Adv. Funct. Mater.* **2016**, *26*, 6402–6417.
[41]W. Han, K. Küpper, P. Hou, W. Akram, H. Eickmeier, J. Hardege, M. Steinhart, H. Schäfer, *ChemSusChem* **2018**, *11*, 3661-3671.
[42] Q. Yuan, Y. Wakisaka, Y. Uemura, T. Wada, H. Ariga-Miwa, S. Takakusagi, K. Asakura, S. R. Brankovic, *J. Phys. Chem. C.*, **2018**, *12*, 229, 16664-16673.
[43]K. S. Kim, N. Winograd, R. E. Davis, *J. Am. Chem. Soc.* **1971**, *93*, 6296-6297.
[44]R. Arrigo, M. Hävecker, M.E. Schuster, C. Ranjan, E. Stotz, A. Knop-Gericke, R. Schlögl, *Angew. Chem. Int. Ed*. **2013**, *52*, 11660-11664.
[45]V. A. Saveleva, V. Papaefthimiou, M. K. Daletou, W. H. Doh, C. Ulhaq-Bouillet, M. Diebold, S. Zafeiratos, E. R. Savinova, *J. Phys. Chem. C* **2016**, *120*, 15930-15940.
[46]J. P. Hoare in Advances in Electrochemistry and Electrochemical Engineering, Vol. 6 (Eds.: P. Delahay, C. W. Tobias), Interscience, New York, (1966) 201– 288.
[47]C. C. Tseung, S. Jasem, *Electrochim. Acta* **1977**, *22*, 31-34.
[48]M. Pourbaix in Atlas d'Equilibres Electrochemiques a 25 8C, Gauthiers-Villars, Paris, (1963).
[49] H. Angerstein-Kozlowka, B.E. Conway, B. Barnett, J. Mozota, *J. Electroanal. Chem*. **1979**, *100*, 417-446.
[50] B. E. Conway, G. Tremiliosi-Filho, G. Jerkiewicz, *J. Electroanal. Chem*. **1991**, *297*, 435-443.
[51] B. E. Conway, G. Jerkiewicz, *J. Electroanal. Chem*. **1992**, *339*, 123-146.
[52] B. E. Conway, *Prog. Surf. Sci.* **1995**, *49*, 331-452.
[53]S. Mitsushima, Y. Koizumi, S. Uzuka, K.-I. Ota, *Electrochim. Acta* **2008**, *54*, 455-460.
[54] M. Tian, C. Cousins, D. Beauchemin, Y. Furuya, A. Ohma, G. Jerkiewicz, *ACS Catal.* **2016**, *6*, 5108-5116.
[55] R. M. Darling, J. P. Meyers, *J. Electrochem. Soc.* **2003**, 150, A1523-A1527.
[56]S. A. Grigoriev, P. Millet, V.N. Fateev, *J. Power Sources* **2008**, *177*, 281-285.
[57]M. Bernt, A. Siebel, H. A. Gasteiger, *J. Electrochem. Soc.* **2018**, *165*, F305-F314.
[58]L. Dubau, L. Castanheira, G. Berthomé, F. Maillard, *Electrochim. Acta* **2013**, *110*, 273– 281.
[59]L. Dubau, M. Lopez-Haro, L. Castanheira, J. Durst, M. Chatenet, P. Bayle-Guillemaud, L. Guétaz, N. Caqué, E. Rossinot, F. Maillard, *Appl. Catal. B: Environmental* **2013**, *142-143*, 801-808.
[60]Z. Zhao, L. Castanheira, L. Dubau, G. Berthomé, A. Crisci, F. Maillard, *J. Power Sources* **2013**, *230*, 236-243.
[61]L. Castanheira, L. Dubau, F. Maillard, *Electrocatal.* **2014**, *5*, 125-135.
[62]L. Castanheira, L. Dubau, M. Mermoux, G. Berthomé, N. Caqué, E. Rossinot, M. Chatenet, F. Maillard, *ACS Catal.* **2014**, *4*, 2258-2267.
[63]L. Dubau, L. Castanheira, M. Chatenet, F. Maillard, J. Dillet, G. Maranzana, S. Abbou, O. Lottin, G. De Moor, A. El Kaddouri, C.

Bas, L. Flandin, E. Rossinot, N. Caqué, *Int. J. Hydrogen Energy* **2014**, *39*, 21902-21914.
[64]L. Dubau, L. Castanheira, F. Maillard, M. Chatenet, O. Lottin, G. Maranzana, J. Dillet, A. Lamibrac, J.-C. Perrin, E. Moukheiber, A. ElKaddouri, G. De Moor, C. Bas, L. Flandin, N. Caqué, *WIRES Energy Environ.* **2014**, *3*, 540-560.